AuPt/3DOM $CoCr_2O_4$: Highly Active Catalysts for the Combustion of Methane

Xiyun Jiang, Yuxi Liu, Jiguang Deng, Xingtian Zhao, Shan Sun, Chengwei Zhai, Fei Peng and Hongxing Dai*

Beijing Key Laboratory for Green Catalysis and Separation, Key Laboratory of Beijing on Regional Air Pollution Control, and Laboratory of Catalysis Chemistry and Nanoscience, Department of Chemistry and Chemical Engineering, College of Environmental and Energy Engineering, Beijing University of Technology, Beijing 100124, China

Abstract: Three-dimensionally ordered macroporous (3DOM) $CoCr_2O_4$ and its supported bimetallic Au_y Pt nanocatalysts ($x$$Au_y$Pt/3DOM $CoCr_2O_4$, x = 0.49, 0.98, and 1.92 wt%; Au/Pt molar ratio (y) = 0.99, 0.98, and 1.01) were prepared using the polymethyl methacrylate-templating and polyvinyl alcohol-protected reduction methods, respectively. Physicochemical properties of the samples were characterized by means of various techniques. Catalytic activities of the $x$$Au_y$Pt/3DOM $CoCr_2O_4$ samples were evaluated for methane combustion. It is found that the 3DOM $CoCr_2O_4$ support possessed a single-phase and cubic spinel-type crystal structure, the $x$$Au_y$Pt/3DOM $CoCr_2O_4$ samples displayed a high-quality 3DOM architecture and a surface area of 32-33 m^2/g, and the Au_yPt nanoparticles (NPs) with a size of 3-5 nm were well dispersed on the 3DOM $CoCr_2O_4$ surface. The loading of an appropriate amount of Au_yPt NPs could enhance the adsorbed oxygen species concentration and low-temperature reducibility of the sample. Among all of the samples, 0.98$Au_{0.98}$Pt/3DOM $CoCr_2O_4$ showed the best catalytic performance: the $T_{10\%}$, $T_{50\%}$, and $T_{90\%}$ (temperatures required for achieving methane conversion of 10, 50, and 90 %, respectively) were 253, 315, and 354 °C at a space velocity of 20,000 mL/(g h). It is concluded that the good activity of 0.98$Au_{0.98}$Pt/3DOM $CoCr_2O_4$ was associated with its highly dispersed $Au_{0.98}$Pt NPs, high adsorbed oxygen species concentration, good low-temperature reducibility, and strong interaction between $Au_{0.98}$Pt NPs and 3DOM $CoCr_2O_4$.

Keywords: Three-dimensionally ordered macropore, spinel-type cobalt chromate, bimetallic gold-platinum nanoparticle, supported noble metal catalyst, methane combustion.

1. INTRODUCTION

Methane is widely used in chemical industries, transportation activities, and private families [1,2]. Methane can induce a strong greenhouse effect with a global warming potential 20 times higher than that of CO_2 [3]. To meet the strict emission regulations, efforts are required to be made in developing efficient strategies for reducing methane emissions. Catalytic combustion is a promising technology that can convert methane into CO_2 and H_2O at low temperatures [4]. Therefore, it is highly desirable to find out heterogeneous catalysts that can efficiently eliminate the emission of methane.

Supported noble metal (e.g., Pd and Pt) catalysts perform well for methane combustion at low temperatures [5]. For example, Hu *et al.* [6] observed a high activity of 5 wt% Pd/Co_3O_4 nanosheets for methane combustion, and assigned the good performance to the existence of a strong interaction between Pd^{2+} and Co_3O_4. Han and coworkers [7] claimed that the good activity of Pd/γ-Al_2O_3 for CH_4 combustion was due to formation of the PdO_x at the top layers above 250 °C. Doping of a less cheap metal to Pd or Pt, one can generate a bimetallic catalyst. Au is an ideal candidate. The doping of Au to Pd or Pt can greatly enhance the catalytic activity and stability. There have been several reports on the use of Au-Pd nanoparticles (NPs) in the oxidation of toluene, alcohols, and methane [8-11]. For instance, Hutchings and coworkers [11] investigated the Au-Pd/TiO_2 catalysts for the oxidation of primary alcohols, and concluded that the Au could act as an electronic promoter for Pd. Chen *et al.* [10] found a promotional effect of Au in the Au-Pd alloy catalyst, and pointed out that the Au could isolate the Pd site. The catalytic performance of the Pd-based materials for methane lean-burn combustion at low temperatures could be enhanced if the Pd was alloyed with other metals (e.g., Pt [12]). The Pt was found to be more active under the rich-burn conditions but less active under lean-burn conditions than the Pd catalysts [13]. Several works [14-18] reported that substituting Pt for Pd could generate a catalyst that exhibited enhanced activity and stability. Transition-metal oxides are usually used as active catalysts and good supports. Among the transition-metal oxide catalysts, Cr-based spinel-type oxides (e.g., $CoCr_2O_4$) show moderate catalytic

*Address correspondence to this author at the Beijing Key Laboratory for Green Catalysis and Separation, Key Laboratory of Beijing on Regional Air Pollution Control, and Laboratory of Catalysis Chemistry and Nanoscience, Department of Chemistry and Chemical Engineering, College of Environmental and Energy Engineering, Beijing University of Technology, Beijing 100124, China; Tel: 8610 6739 6118; Fax: 8610 6739 1983; E-mail: hxdai@bjut.edu.cn

E-ISSN: 2410-3624/17

activities in methane combustion [19-21]. For example, Li and coworkers [20] reported that cobalt–chromium oxide with a Co/Cr atomic ratio of 1 : 2 performed well for CH_4 combustion.

In recent years, three-dimensionally ordered macroporous (3DOM) materials have gained much attention in catalysis, because they have several advantages of high surface areas, easy mass transfer, and suitability for dispersion of active components. To the best of our knowledge, there have so far been no reports in the literature on the preparation and catalytic activities of 3DOM $CoCr_2O_4$-supported Au_yPt NPs for methane combustion. In this work, we adopted the polymethyl methacrylate (PMMA)-templating and polyvinyl alcohol (PVA)-protected reduction strategies to generate the 3DOM $CoCr_2O_4$ and xAu$_y$Pt/3DOM $CoCr_2O_4$ nanocatalysts, characterized their physicochemical properties, and evaluated their catalytic activities for methane combustion. It is found that the 0.98 wt% $Au_{0.98}Pt$/3DOM $CoCr_2O_4$ sample performed the best for the addressed reaction.

2. EXPERIMENTAL

2.1. Catalyst Preparation

The well-arrayed PMMA microspheres with an average diameter of ca. 300 nm were synthesized according to procedures described elsewhere [22].

The 3DOM $CoCr_2O_4$ support was fabricated using the PMMA-templating method. In a typical procedure, 6.66 mmol of $Co(NO_3)_2{\cdot}6H_2O$ and 13.32 mmol of $Cr(NO_3)_3{\cdot}9H_2O$ were dissolved in 10 mL of poly(ethylene glycol) (MW = 400 g/mol) and methanol solution (poly(ethylene glycol)/methanol volumetric ratio = 1.0 : 9.0) at room temperature (RT) under stirring for 30 min to obtain a transparent solution. Then, 2.00 g of the PMMA template was soaked in the above precursor solution for ca. 30 min. After that, the mixture was filtered and dried at RT for 48 h. The as-obtained powders were calcined in N_2 (100 mL/min) at a ramp of 1 ^oC/min from RT to 300 ^oC and maintained at 300 ^oC for 2 h, then cooled to RT, calcined in air (100 mL/min) at a ramp of 1 ^oC/min from RT to 300 ^oC and maintained at 300 ^oC for 2 h, and finally heated to 500 ^oC and maintained at 500 ^oC for 4 h, thus obtaining the 3DOM $CoCr_2O_4$ support.

The 3DOM $CoCr_2O_4$-supported Au, Pt, and Au_yPt (xAu/3DOM $CoCr_2O_4$, xPt/3DOM $CoCr_2O_4$, and xAu$_y$Pt/3DOM $CoCr_2O_4$) samples were prepared using the PVA-protected reduction strategy. The typical preparation procedure is as follows: A certain amount of PVA aqueous solution (2.00 g/L) was added to $HAuCl_4$ (1.50 mmol/L) aqueous solution, H_2PtCl_6 (1.50 mmol/L) aqueous solution, and $HAuCl_4$ (1.50 mmol/L) and H_2PtCl_6 (1.50 mmol/L) mixed aqueous solution (Au/PVA mass ratio = 1.5 : 1.0 (mg/mg), Pt/PVA mass ratio = 1.5 : 1.0 (mg/mg); the Au/Pt theoretical molar ratio = 1.0; and the Au, Pt, and Au_yPt theoretical loadings (x) were 0.50, 0.50, 0.50, 1.00, and 2.00 wt%, respectively) in a ice bath under vigorous stirring for 30 min. Then, an appropriate amount of $NaBH_4$ aqueous solution (2.00 g/L) was quickly injected into the mixed noble metal aqueous solution, generating a dark-brown sol. Subsequently, 0.30 g of the 3DOM $CoCr_2O_4$ support was then added to the dark-brown sol and vigorously stirred for 6 h. Afterwards, the mixture solution was filtered and washed with deionized water until there was no Cl^- ions in the supernatant were detected using an $AgNO_3$ aqueous solution (0.10 mol/L). The obtained wet solid was dried at 80 ^oC for 10 h, and calcined in a muffle furnace at a ramp of 1 ^oC/min from RT to 500 ^oC and maintained at this temperature for 4 h, thus obtaining the xAu$_y$Pt/3DOM $CoCr_2O_4$ samples. The results of inductively coupled plasma atomic emission spectroscopic (ICP-AES) investigations reveal that the actual loadings of noble metals were 0.49, 0.48, 0.49, 0.98, and 1.92 wt% in xAu/3DOM $CoCr_2O_4$, xPt/3DOM $CoCr_2O_4$, and xAu$_y$Pt/3DOM $CoCr_2O_4$, respectively, and the corresponding actual Au/Pt molar ratios in xAu$_y$Pt/3DOM $CoCr_2O_4$ were 0.99, 0.98, and 1.01.

All chemicals (A.R. in purity) were purchased from Beijing Chemical Reagent Company and used without further purification.

2.2. Catalyst Characterization

The actual noble metal loadings in the samples were measured using the ICP-AES technique on a Thermo Electron IRIS Intrepid ER/S spectrometer. X-ray diffraction (XRD) patterns of the samples were determined on a Bruker D8 Advance diffractometer with Cu Kα radiation and nickel filter (λ = 0.15406 nm). Scanning electron microscopic (SEM) images of the samples were taken on a Gemini Zeiss Supra 55 equipment (operating at 10 kV). Transmission electron microscopic (TEM) images of the samples were recorded on a JEOL-2010 apparatus (operating at 200 kV). BET (Brunauer-Emmett-Teller) surface areas and pore-size distributions of the samples were determined via N_2 adsorption at –196 ^oC on a Micromeritics ASAP

2020 analyzer, with the samples being out gassed at 250 °C for 2 h under vacuum before measurement. X-ray photoelectron spectroscopy (XPS, ESCALAB 250 Xi, Thermo Fisher Scientific) was used to determine the Co 2p, Cr 2p, O 1s, Au 4f, Pt 4f, and C 1s binding energies (BEs) of surface species using Al Kα ($h\nu$ = 1486.6 eV) as the excitation source.

H_2 temperature-programmed reduction (H_2-TPR) experiments of the samples were conducted on a chemical adsorption analyzer (Autochem II 2920, Micromeritics). Before H_2-TPR measurement, ca. 50 mg of the sample (40-60 mesh) was charged to a quartz fixed-bed U-shaped microreactor (i.d. = 4 mm) and pretreated in O_2 flow (20 mL/min) at 300 °C for 1 h. After being cooled to RT in the same atmosphere, the sample was purged with He (30 mL/min) for 15 min. Finally, the pretreated sample was exposed to a 5% H_2-95% Ar (*v*/*v*) mixture (50 mL/min) and heated at a ramp of 10 °C/min from RT to 700 °C. The change in effluent H_2 concentration was monitored online by the chemical adsorption analyzer. The reduction peak was calibrated against that of the complete reduction of a standard CuO (Aldrich, 99.995%) sample.

2.3. Catalytic Evaluation

Catalytic activities of the samples were evaluated in a continuous flow fixed-bed quartz tubular microreactor (i.d. = 6.0 mm). 50 mg of the sample (40-60 mesh) was diluted with 0.25 g of quartz sands (40-60 mesh). Prior to the measurement, the sample was pretreated in an O_2 flow of 20 mL/min at 300 °C for 1 h. After being cooled to a given temperature, the reactant gas containing methane was passed through the catalyst bed. The reactant mixture gas was 2.5 vol% CH_4 + 20 vol% O_2 + 77.5 vol% N_2 (balance), and the total flow was 16.7 mL/min, giving a space velocity (SV) of ca. 20,000 mL/(g h). In the case of water vapor introduction, 5.0 vol% H_2O was introduced by passing the feed stream through a water saturator at a certain temperature. In the case of CO_2 introduction, 2.5 or 5.0 vol% CO_2 from a CO_2 cylinder (balanced with N_2) was introduced to the reaction system through a mass flow controller. Reactants and products were analyzed online by gas chromatography (GC-14C, Shimadzu) equipped with a flame ionization detector (FID) and a thermal conductivity detector (TCD), using a stabilwax column (30 m in length) for methane separation and a Carboxen 1000 column (3 m in length) for permanent gas detection. The balance of carbon throughout the catalytic system was estimated to be 99.5 ± 1.5%. Catalytic activities of the samples were evaluated using the temperatures ($T_{10\%}$, $T_{50\%}$, and $T_{90\%}$) required for achieving methane conversions of 10, 50, and 90%, respectively. CH_4 conversion was defined as $(c_{inlet} - c_{outlet})/c_{inlet} \times 100\%$, where the c_{inlet} and c_{outlet} are CH_4 concentrations of the inlet and outlet feed stream, respectively.

3. RESULTS AND DISCUSSION

3.1. Physical Properties of the Samples

According to the results (Table **1**) of ICP-AES characterization, the *x*Au/3DOM $CoCr_2O_4$, *x*Pt/3DOM $CoCr_2O_4$, and *x*Au$_y$Pt/3DOM $CoCr_2O_4$ samples can be denoted as 0.49Au/3DOM $CoCr_2O_4$, 0.48Pt/3DOM

Table 1: Surface Areas, Pore Diameters, Pore Volumes, Average Noble Metal Particle Sizes, Nominal and Actual Noble Metal Contents, and Actual Au/Pt Molar Ratios of the As-Prepared Samples

Sample	Surface area (m^2/g)	Pore diameter[a] (nm)	Pore volume (cm^3/g)	Average noble metal particle size[b] (nm)	Nominal noble metal content (wt%)	Actual noble metal content[c] (wt%)	Actual Au/Pt molar ratio[c]
3DOM $CoCr_2O_4$	33.2	120–180	0.029	–	–	–	–
0.49Au/3DOM $CoCr_2O_4$	34.5	120–180	0.030	3.4	0.50	0.49	–
0.48Pt/3DOM $CoCr_2O_4$	34.3	120–180	0.030	3.5	0.50	0.48	–
0.49$Au_{0.99}$Pt/3DOM $CoCr_2O_4$	32.8	120–180	0.029	2.7	0.50	0.49	0.99
0.98$Au_{0.98}$Pt/3DOM $CoCr_2O_4$	33.1	120–180	0.029	3.0	1.00	0.98	0.98
1.92$Au_{1.01}$Pt/3DOM $CoCr_2O_4$	32.1	120–180	0.028	4.5	2.00	1.92	1.01

[a] Data were estimated according to the SEM images of the samples;

[b] Data were estimated according to the noble metal particles in the TEM images of the samples;

[c] Data were determined by the ICP-AES technique.

$CoCr_2O_4$, $0.49Au_{0.99}Pt$/3DOM $CoCr_2O_4$, $0.98Au_{0.98}$ Pt/3DOM $CoCr_2O_4$, and $1.92Au_{1.01}Pt$/3DOM $CoCr_2O_4$, respectively.

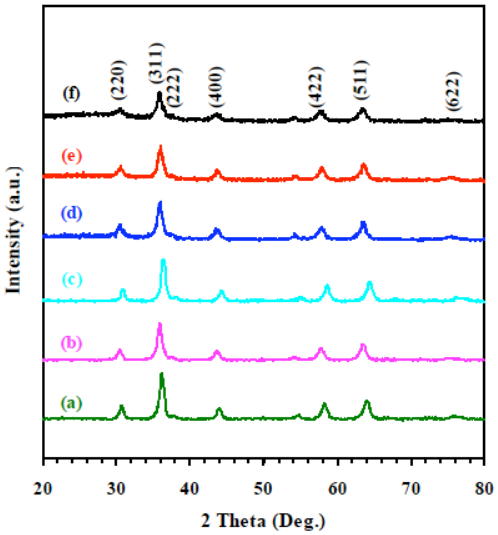

Figure 1: XRD patterns of (a) 3DOM $CoCr_2O_4$, (b) 0.49Au/3DOM $CoCr_2O_4$, (c) 0.48Pt/3DOM $CoCr_2O_4$, (d) $0.49Au_{0.99}Pt$/3DOM $CoCr_2O_4$, (e) $0.98Au_{0.98}Pt$/3DOM $CoCr_2O_4$, and (f) $1.92Au_{1.01}Pt$/3DOM $CoCr_2O_4$.

Figure **1** illustrates the XRD patterns of the as-fabricated samples. By comparing the XRD patterns of these samples with that of the standard $CoCr_2O_4$ sample (JCPDS PDF # 22-1084), one can realize that the single-phase $CoCr_2O_4$ in the 3DOM $CoCr_2O_4$ and its supported noble metal samples was of cubic spinel-type crystal structure, and all of the Bragg diffraction peaks were well indexed (Figure **1f**). The loading of Au, Pt or Au_yPt NPs did not give rise to a change in crystal phase of 3DOM $CoCr_2O_4$. No crystal phases assignable to the Au, Pt or Au_yPt NPs were recorded, demonstrating that the noble metal NPs were uniformly dispersed on the surface of 3DOM $CoCr_2O_4$. No detection of noble metal phases might be due to low loadings and high dispersion of noble metal NPs. It should be noted that an alloy of Au_yPt might be formed in Au_yPt NPs of the Au_yPt/3DOM $CoCr_2O_4$ samples due to the similarity in synthesis method of Au_yPt NPs and Au-Pd NPs [23-25], in which an Au-Pd alloy was confirmed to be generated. Figure **2** shows the SEM images of the samples. It is clearly observed that the 3DOM $CoCr_2O_4$ and its supported noble metal samples possessed a high-quality 3DOM structure with a macropore size of 120-180 nm. The loading of noble metal NPs did not induce a significant alteration in macropore structure of 3DOM $CoCr_2O_4$. As shown in the TEM images (Figure **3**), the Au, Pt or Au_yPt NPs were uniformly deposited on the surface of 3DOM $CoCr_2O_4$. The sizes of Au, Pt or Au_yPt NPs were in the range of 3-5 nm. By statistically analyzing the sizes of

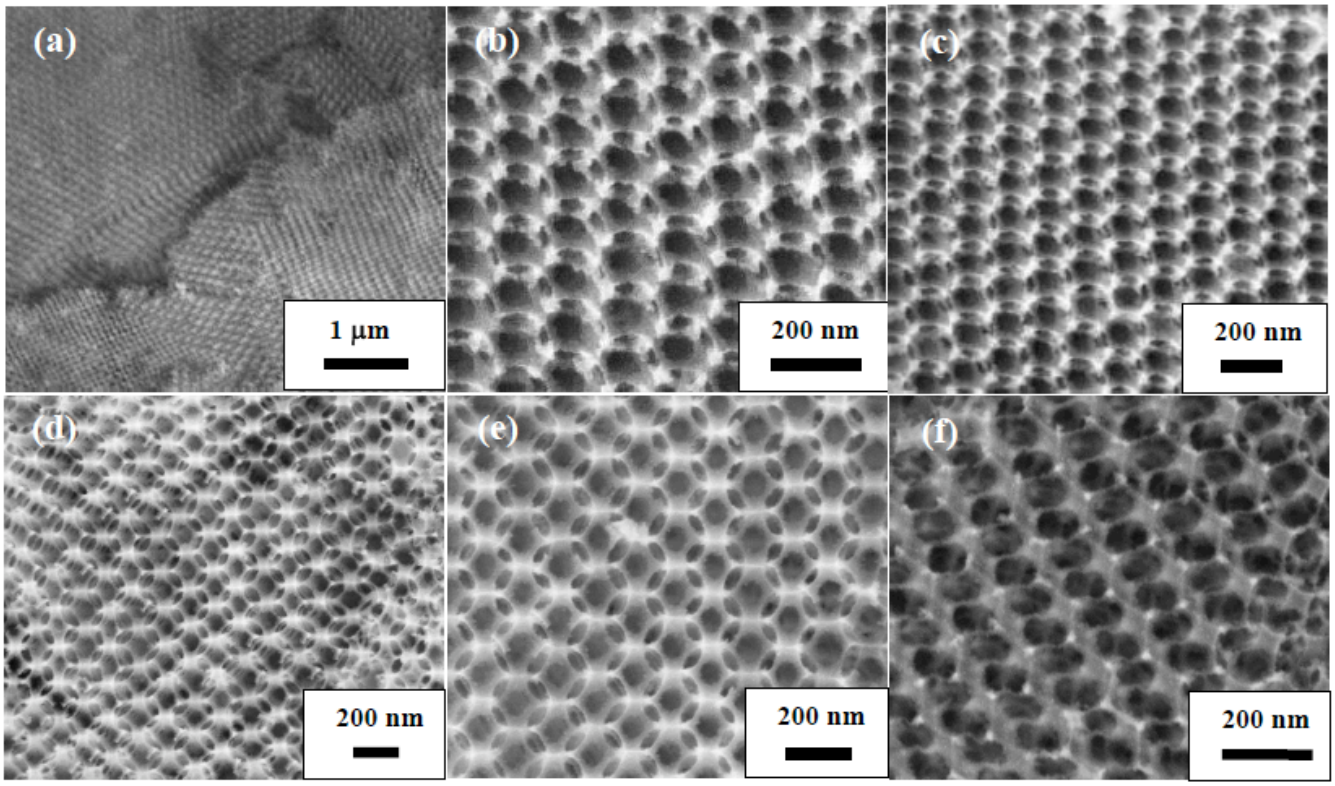

Figure 2: SEM images of (**a**) 3DOM $CoCr_2O_4$, (**b**) 0.49Au/3DOM $CoCr_2O_4$, (**c**) 0.48Pt/3DOM $CoCr_2O_4$, (**d**) $0.49Au_{0.99}Pt$/3DOM $CoCr_2O_4$, (**e**) $0.98Au_{0.98}Pt$/3DOM $CoCr_2O_4$, and (**f**) $1.92Au_{1.01}Pt$/3DOM $CoCr_2O_4$.

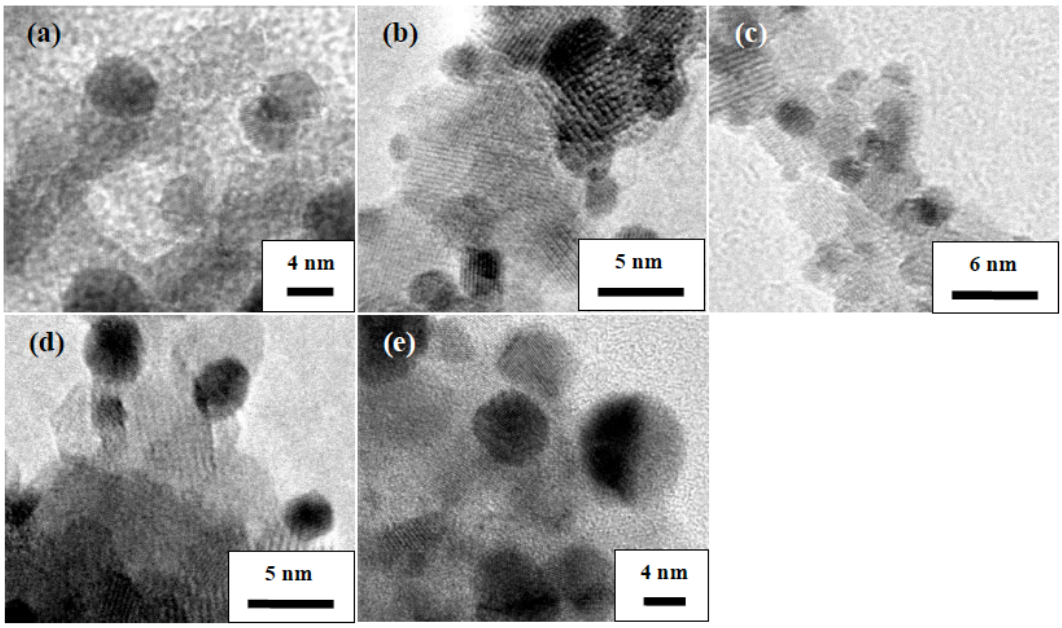

Figure 3: TEM images of (a) 0.49Au/3DOM $CoCr_2O_4$, (b) 0.48Pt/3DOM $CoCr_2O_4$, (c) $0.49Au_{0.99}Pt$/3DOM $CoCr_2O_4$, (d) $0.98Au_{0.98}Pt$/3DOM $CoCr_2O_4$, and (e) $1.92Au_{1.01}Pt$/3DOM $CoCr_2O_4$.

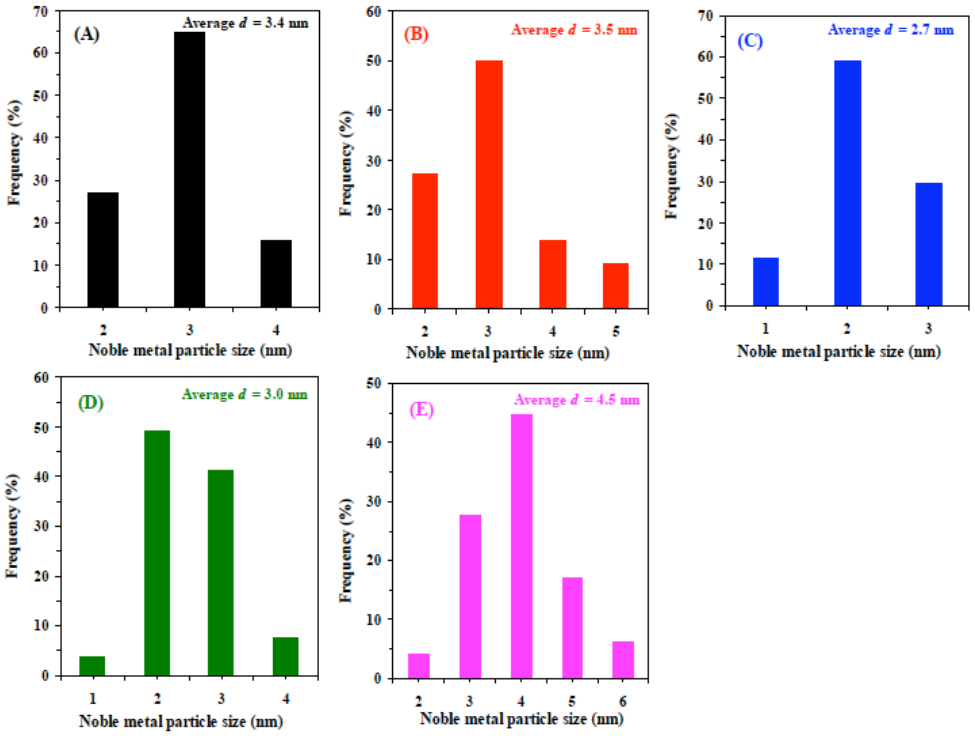

Figure 4: Noble metal particle size distributions of (A) 0.49Au/3DOM $CoCr_2O_4$, (B) 0.48Pt/3DOM $CoCr_2O_4$, (C) $0.49Au_{0.99}Pt$/3DOM $CoCr_2O_4$, (D) $0.98Au_{0.98}Pt$/3DOM $CoCr_2O_4$, and (E) $1.92Au_{1.01}Pt$/3DOM $CoCr_2O_4$.

100 particles in the TEM images of the supported noble metal samples, one can obtain the particle size distributions of noble metal NPs, as shown in Figure **4**. The average sizes of noble metal NPs in 0.49Au/3DOM $CoCr_2O_4$, 0.48Pt/3DOM $CoCr_2O_4$, $0.49Au_{0.99}Pt$/3DOM $CoCr_2O_4$, $0.98Au_{0.98}Pt$/3DOM $CoCr_2O_4$, and $1.92Au_{1.01}Pt$/3DOM $CoCr_2O_4$ were 3.4, 3.5, 2.7, 3.0, and 4.5 nm, respectively.

Figure **5** shows the N_2 adsorption-desorption isotherms and pore-size distributions of the samples, and their textural properties are summarized in Table **1**.

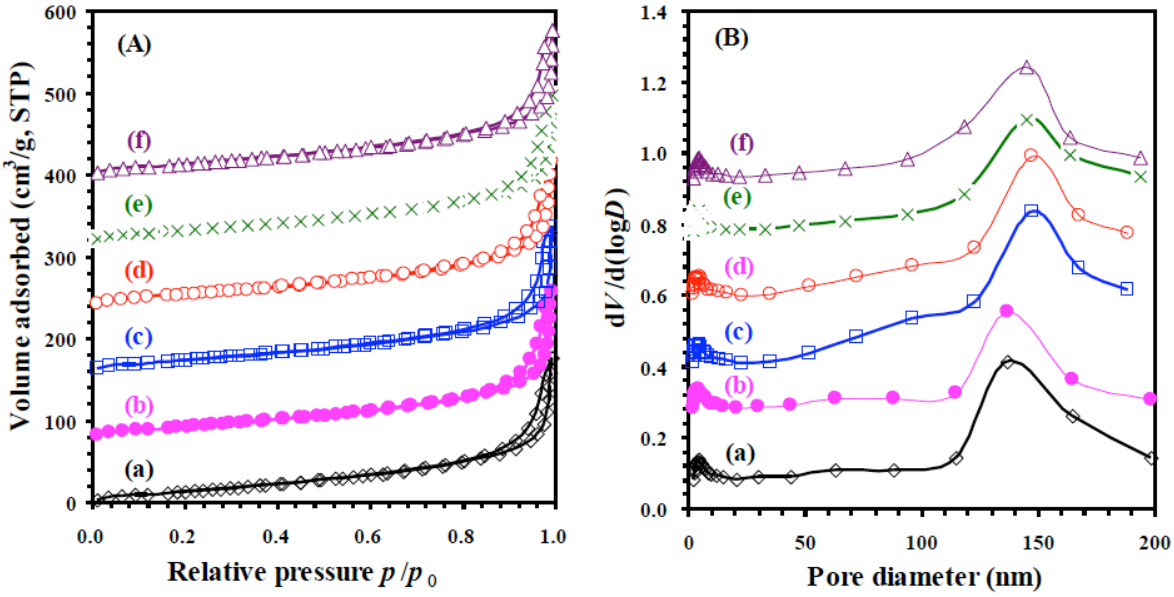

Figure 5: (**A**) N_2 adsorption-desorption isotherms and, (**B**) pore-size distributions of, (a) 3DOM $CoCr_2O_4$, (b) 0.49Au/3DOM $CoCr_2O_4$, (c) 0.48Pt/3DOM $CoCr_2O_4$, (d) $0.49Au_{0.99}Pt$/3DOM $CoCr_2O_4$, (e) $0.98Au_{0.98}Pt$/3DOM $CoCr_2O_4$, and (f) $1.92Au_{1.01}Pt$/3DOM $CoCr_2O_4$.

It is observed from Figure **5A** that all of the samples showed a type II isotherm with a type H3 hysteresis loop in the relative pressure (p/p_0) range of 0.8-1.0, indicating the presence of a macroporous structure in each sample. From the pore-size distributions of the samples (Figure **5B**), one can see that each sample possessed a pore-size distribution in the ranges of 2-10 and 100-200 nm, respectively. The mesopores or nanocaves in the pore size of 2-10 nm on the skeletons of 3DOM $CoCr_2O_4$ might be formed after the poly(ethylene glycol)-containing precursor was calcined. BET surface area and pore volume of 3DOM $CoCr_2O_4$ were 33.2 m^2/g and 0.029 cm^3/g, respectively. After loading of Au, Pt or Au_yPt NPs, there were no significant changes in surface area and pore volume (32.1-34.5 m^2/g and 0.028-0.030 cm^3/g, respectively).

3.2. Surface Element composition, Metal Oxidation State, and Oxygen Species

XPS is an effective technique to investigate the surface element compositions, metal oxidation states, and adsorbed species of a catalyst. Figure **6** shows the Co $2p_{3/2}$, Cr $2p_{3/2}$, O 1s, Au 4f, and Pt 4f XPS spectra of the samples. There was an asymmetrical Co $2p_{3/2}$ XPS signal of each sample that could be decomposed to two components at BE = 780.8 and 783.4 eV (Figure **6A**), attributable to the surface Co^{3+} and Co^{2+} species [26], respectively. The presence of surface Co^{2+} species in the samples was verified by the appearance of a satellite at BE = 787.3 eV. The surface Co^{3+}/Co^{2+} molar ratios of the samples are summarized in Table **2**. The surface Co^{3+}/Co^{2+} molar ratio significantly decreased from 2.92 to 2.42–2.80 after the loading of Au, Pt or Au_yPt NPs. In other words, the 3DOM $CoCr_2O_4$ in the supported noble metal samples would possess higher oxygen vacancy density in the surface vicinity of 3DOM $CoCr_2O_4$ [27]. The asymmetrical Cr $2p_{3/2}$ XPS spectrum of each sample was decomposed into three components at BE = 575.4, 576.6, and 578.3 eV (Figure **6B**) that were assigned to the surface $Cr(OH)_3$ or Cr_2O_3 [28], Cr^{3+} (occupied octahedral sites) [20,29], and Cr^{6+} [20,30,31] species, respectively. The Cr^{6+}/Cr^{3+} molar ratio decreased from 0.53 to 0.44–0.52 (Table **2**) when the noble metal NPs were loaded on the surface of 3DOM $CoCr_2O_4$.

As shown in Figure **6C**, the asymmetric O 1s XPS signal could be deconvoluted to three components at BE = 530.1, 531.5, and 532.9 eV that were ascribed to the surface lattice oxygen (O_{latt}), adsorbed oxygen (O_{ads}, e.g., O_2^-, O_2^{2-} or O^-), and adsorbed water or carbonate species [32, 33], respectively. It has been reported that the O_{ads} species played an important role in the combustion of organic compounds [32]. With the loading of noble metal NPs, the O_{ads}/O_{latt} molar ratio increased, with the $0.98Au_{0.98}Pt$/3DOM $CoCr_2O_4$ sample possessing the highest O_{ads}/O_{latt} molar ratio (0.63).

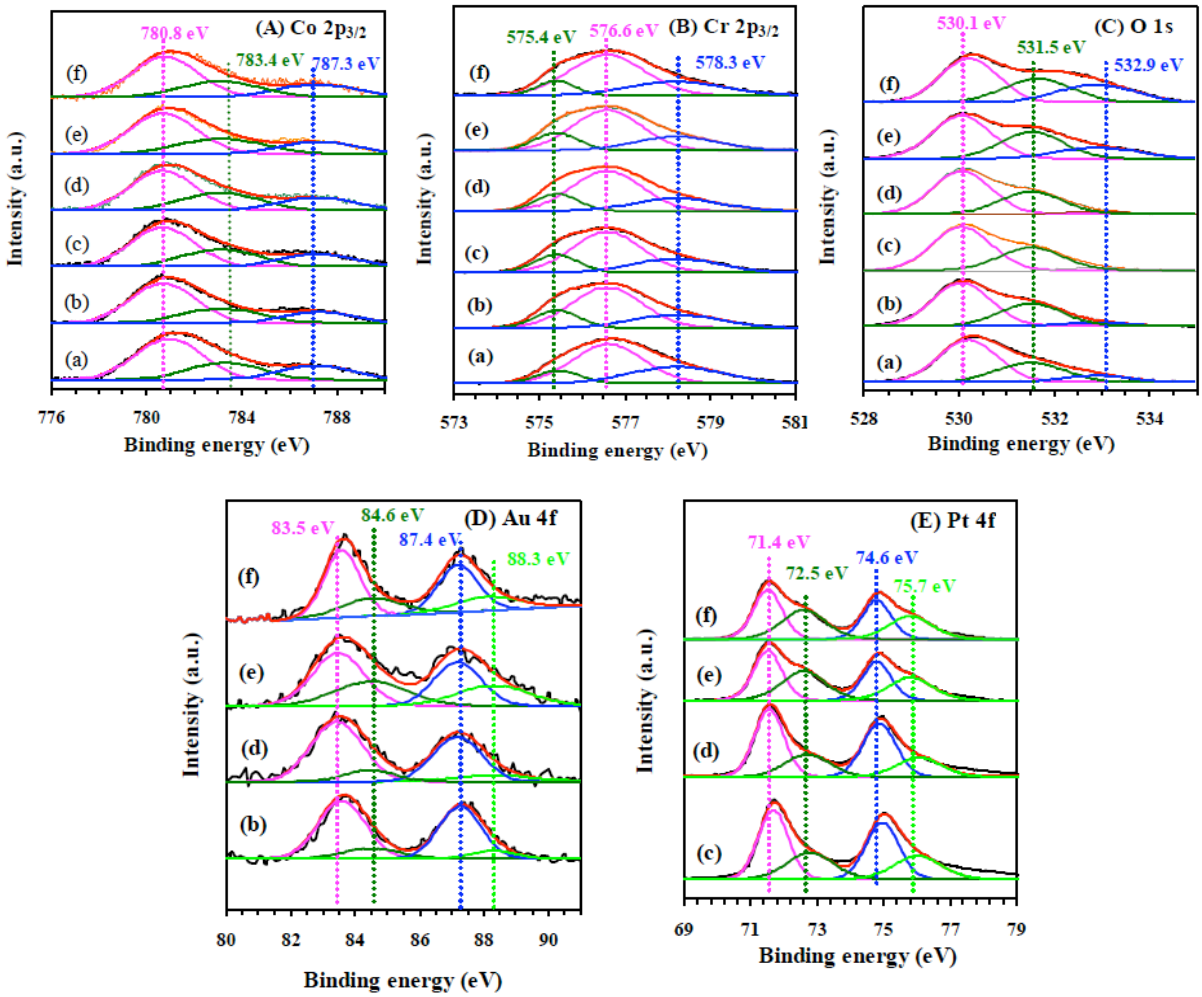

Figure 6: (**A**) Co $2p_{3/2}$, (**B**) Cr $2p_{3/2}$, (**C**) O 1s, (**D**) Au 4f, and (**E**) Pt 4f XPS spectra of (a) 3DOM $CoCr_2O_4$, (b) 0.49Au/3DOM $CoCr_2O_4$, (c) 0.48Pt/3DOM $CoCr_2O_4$, (d) $0.49Au_{0.99}Pt$/3DOM $CoCr_2O_4$, (e) $0.98Au_{0.98}Pt$/3DOM $CoCr_2O_4$, and (f) $1.92Au_{1.01}Pt$/3DOM $CoCr_2O_4$.

Table 2: Surface Element Compositions and H_2 Consumption of the Samples

Sample	Co^{3+}/Co^{2+} molar ratio (mol/mol)	Cr^{6+}/Cr^{3+} molar ratio (mol/mol)	O_{ads}/O_{latt} molar ratio (mol/mol)	$Au^{\delta+}/Au^0$ molar ratio (mol/mol)	Pt^{4+}/Pt^0 molar ratio (mol/mol)	H_2 consumption below 400 °C[a] (mmol/g)
3DOM $CoCr_2O_4$	2.92	0.53	0.52	–	–	0.25
0.49Au/3DOM $CoCr_2O_4$	2.80	0.48	0.53	0.16	–	0.19
0.48Pt/3DOM $CoCr_2O_4$	2.62	0.46	0.54	–	0.68	0.26
$0.49Au_{0.99}Pt$/3DOM $CoCr_2O_4$	2.56	0.47	0.56	0.22	0.56	0.29
$0.98Au_{0.98}Pt$/3DOM $CoCr_2O_4$	2.42	0.44	0.63	0.35	0.78	0.52
$1.92Au_{1.01}Pt$/3DOM $CoCr_2O_4$	2.48	0.52	0.55	0.28	0.76	0.74

[a] Data were estimated by quantitatively analyzing the reduction peaks in the H_2-TPR profiles.

The Au 4f XPS spectrum of each sample could be decomposed into four components at BE = 83.5, 84.6, 87.4, and 88.3 eV (Figure **6D**). The components at BE = 83.5 and 87.4 eV were assignable to the surface metallic gold (Au^0) species, while the ones at BE = 84.6 and 88.3 eV were attributable to the surface oxidized

gold ($Au^{\delta+}$) species [23, 34]. As shown in Figure **6E**, the Pt 4f spectrum of each sample could be deconvoluted into four components at BE = 71.4, 72.5, 74.6, and 75.7 eV. The components at BE = 71.4 and 74.6 eV were ascribed to the surface metallic platinum (Pt^0) species, whereas the ones at BE = 72.5 and 75.7 eV were attributed to the surface oxidized platinum (Pt^{4+}) species [35]. Apparently, the $Au^{\delta+}/Au^0$ or Pt^{4+}/Pt^0 molar ratio increased but the Co^{3+}/Co^{2+} and Cr^{6+}/Cr^{3+} molar ratios decreased with the loading of Au_yPt NPs, a result possibly due to the strong interaction between noble metal NPs and 3DOM $CoCr_2O_4$ (Au^0 or Pt^0 + Co^{3+} (Cr^{6+}) → $Au^{\delta+}$ or Pt^{4+} + Co^{2+} (Cr^{3+})) [23,36].

3.3. Reducibility

H_2-TPR is an effective technique to investigate the reducibility of a catalyst. Figure **7A** illustrates the H_2-TPR profiles of the samples. For the 3DOM $CoCr_2O_4$ sample, there were three reduction peaks at 282 and 467 °C and above 620 °C. The reduction peaks at 282 and 467 °C were due to the reduction of Cr^{6+} to Cr^{3+} and/or Co^{3+} to Co^{2+} on the surface and in the bulk of 3DOM $CoCr_2O_4$ [30, 37], respectively, whereas the reduction peak above 620 °C was due to the reduction of Co^{2+} to the metallic Co^0 [38]. After loading of Au, Pt or Au_yPt NPs, the reduction peaks of the samples shifted to lower temperatures. Such a significant shift in the first reduction peak was associated with the promotional reduction of Cr^{6+} to Cr^{3+} and/or Co^{3+} to Co^{2+} by the dissociated adsorption of H_2 molecules on the surface of noble metal NPs in the samples. Therefore, the reduction peaks at 51-122 and 252-259 °C could be attributed to the reduction of Cr^{6+} to Cr^{3+} and/or Co^{3+} to Co^{2+} as well as the reduction of cationic Au or Pd and surface O_{ads} species, whereas the reduction peaks at 470-487 and 615-637 °C or above 600 °C were ascribed to the reduction of bulk Cr^{6+} to Cr^{3+} and Co^{2+} to Co^0. After quantitative analysis on the reduction peaks in the H_2-TPR profiles, the H_2 consumption (Table **2**) of the samples can be obtained. The H_2 consumption of the xAu_yPt/3DOM $CoCr_2O_4$ samples increased with the loading of Au_y Pt NPs. Generally speaking, the H_2 consumption refers to the H_2 amount consumed during the reduction process, whereas the initial H_2 consumption rate refers to the H_2 consumption rate at the initial reduction stage (less than 25% oxygen in the sample is consumed for the first reduction peak [39]) of a sample. Usually, there is no direct relation between H_2 consumption and initial H_2 consumption rate, but the latter can be used to evaluate the low-temperature reducibility of a sample. Figure **7B** shows the initial H_2 consumption rate versus inverse temperature of the samples. Obviously, the low-temperature reducibility decreased in the order of $0.98Au_{0.98}Pt$/3DOM $CoCr_2O_4$ > $1.92Au_{1.01}Pt$/3DOM $CoCr_2O_4$ > 0.48Pt/3DOM $CoCr_2O_4$ > $0.49Au_{0.99}$ Pt/3DOM $CoCr_2O_4$ > 0.49Au/3DOM $CoCr_2O_4$ > 3DOM $CoCr_2O_4$, which was in basic agreement with the sequence in catalytic activity (shown below), except that the low-temperature reducibility of 0.48Pt/3DOM $CoCr_2O_4$ was lower than that of $1.92Au_{1.01}Pt$/3DOM $CoCr_2O_4$, which might be due to the contribution of a much higher noble metal loading and additional oxidized Au species in the latter sample.

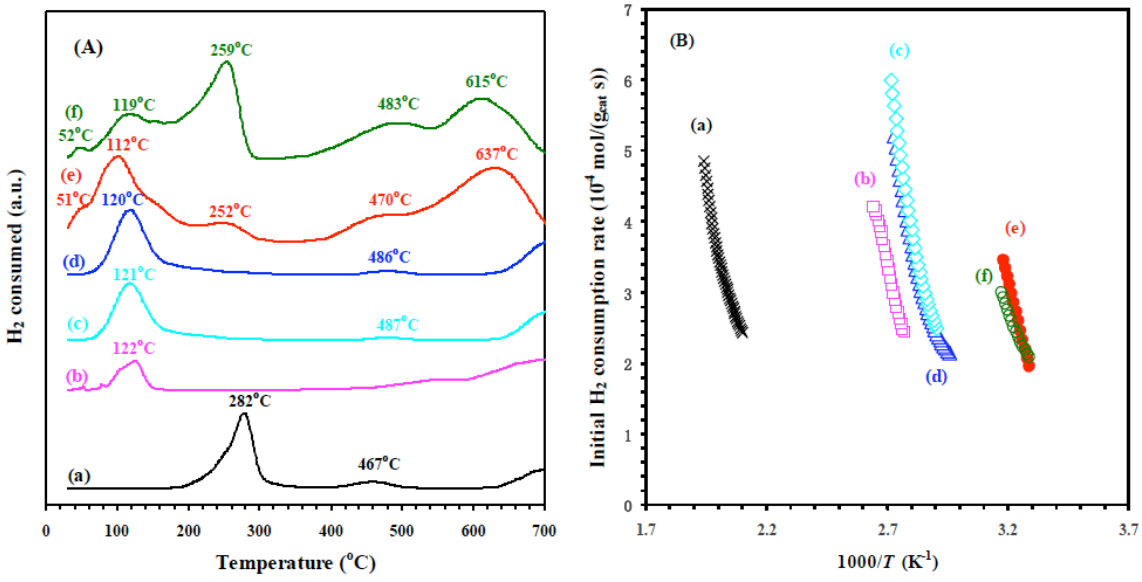

Figure 7: (**A**) H_2-TPR profiles and (**B**) initial H_2 consumption rate of, (a) 3DOM $CoCr_2O_4$, (b) 0.49Au/3DOM $CoCr_2O_4$, (c) 0.48Pt/3DOM $CoCr_2O_4$, (d) $0.49Au_{0.99}Pt$/3DOM $CoCr_2O_4$, (e) $0.98Au_{0.98}Pt$/3DOM $CoCr_2O_4$, and (f) $1.92Au_{1.01}Pt$/3DOM $CoCr_2O_4$.

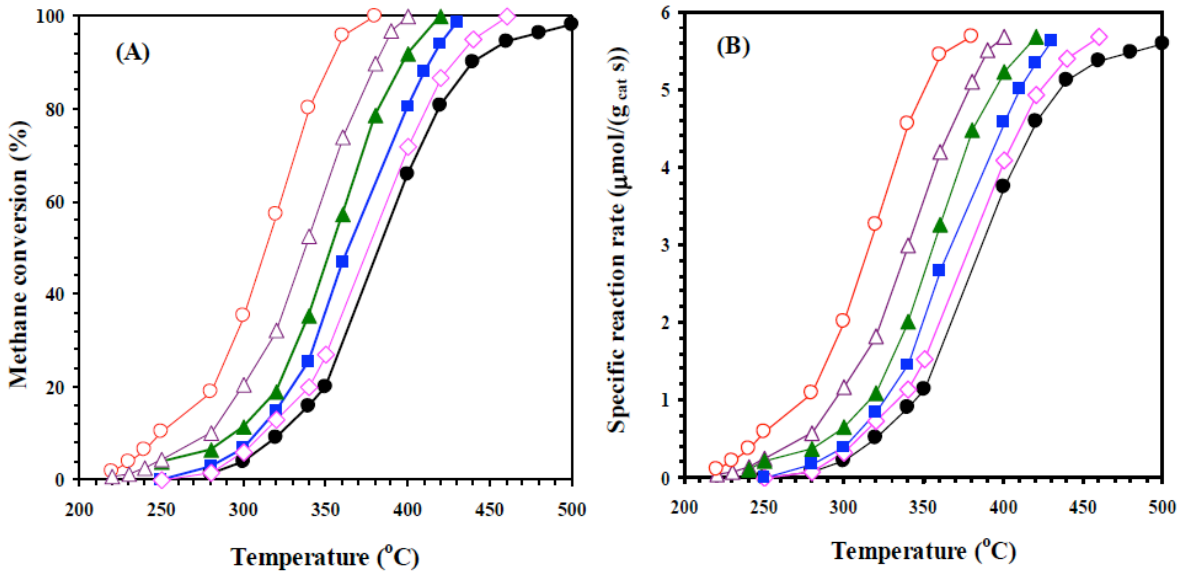

Figure 8: (A) Methane conversion and (B) specific reaction rate as a function of temperature over (●) 3DOM $CoCr_2O_4$, (◇) 0.49Au/3DOM $CoCr_2O_4$, (△) 0.48Pt/3DOM $CoCr_2O_4$, (■) $0.49Au_{0.99}Pt$/3DOM $CoCr_2O_4$, (○) $0.98Au_{0.98}Pt$/3DOM $CoCr_2O_4$, and (▲) $1.92Au_{1.01}Pt$/3DOM $CoCr_2O_4$ at SV = 20,000 mL/(g h).

3.4. Catalytic Performance

In the blank experiment (only quartz sands were loaded in the microreactor), there were no significant methane conversions (< 1%) at temperature < 500 °C and SV = 20,000 mL/(g h). In other words, no considerable gas-phase reaction existed in the catalytic system. Figure **8A** shows the catalytic activities of the samples for methane combustion. To better compare the activities of all of the samples, we use the reaction temperatures ($T_{10\%}$, $T_{50\%}$, and $T_{90\%}$) at methane conversion = 10, 50, and 90%, respectively, as summarized in Table **3**. It is observed that the 3DOM $CoCr_2O_4$-supported noble metal samples ($T_{10\%}$ = 253-313 °C, $T_{50\%}$ = 315-387 °C, and $T_{90\%}$ = 354-428 °C) exhibited better catalytic activities than the 3DOM $CoCr_2O_4$ support ($T_{10\%}$ = 325 °C, $T_{50\%}$ = 393 °C, and $T_{90\%}$ = 441 °C), indicating that the loading of noble metal NPs was beneficial for the enhancement in performance of the sample. Among these samples, the $0.98Au_{0.98}Pt$/3DOM $CoCr_2O_4$ sample showed the highest activity: $T_{10\%}$ = 253 °C, $T_{50\%}$ = 315 °C, and $T_{90\%}$ = 354 °C at SV = 20,000 mL/(g h). Compared to the other samples, $0.98Au_{0.98}Pt$/3DOM $CoCr_2O_4$ possessed higher surface O_{ads}/O_{latt}, $Au^{\delta+}/Au^0$, and Pt^{4+}/Pt^0 molar ratios (Table **2**). It was reported that a larger amount of surface O_{ads} species benefits the combustion of organics [40], and higher surface $Au^{\delta+}$ and Pt^{4+} concentrations could improve the low-temperature reducibility (Figure **7**). Therefore, the best catalytic

Table 3: Catalytic Activities and Specific Reaction Rates at 340 °C of the Samples at SV = 20,000 mL/(g h)

Sample	Methane Combustion Activity			Methane Combustion at 340 °C		
	$T_{10\%}$ (°C)	$T_{50\%}$ (°C)	$T_{90\%}$ (°C)	Specific Reaction Rate (μmol/(g_{cat} s))	Specific Reaction Rate (μmol/(g_{Au} s))	Specific Reaction Rate (μmol/(g_{Pt} s))
3DOM $CoCr_2O_4$	325	393	441	0.91	–	–
0.49Au/3DOM $CoCr_2O_4$	313	387	428	1.14	232	–
0.48Pt/3DOM $CoCr_2O_4$	280	349	381	3.02	–	628
$0.49Au_{0.99}Pt$/3DOM $CoCr_2O_4$	309	365	414	1.48	607	601
$0.98Au_{0.98}Pt$/3DOM $CoCr_2O_4$	253	315	354	4.56	939	920
$1.92Au_{1.01}Pt$/3DOM $CoCr_2O_4$	295	353	397	1.99	206	209

performance of $0.98Au_{0.98}Pt$/3DOM $CoCr_2O_4$ was associated with its highest concentrations of O_{ads} and oxidized noble metal species as well as low-temperature reducibility.

It is well known that there are several kinds of active sites (e.g., noble metal, transition-metal mixed oxide, and interface between noble metal NPs and transition-metal mixed oxide) in the reducible mixed metal oxide-supported noble metal catalysts. Hence, it is difficult to calculate the turnover frequencies. According to the activity data and amounts of catalysts and noble metals in the samples, we can calculate specific reaction rates normalized per gram of catalyst, Au or Pt, as shown in Figure **8B** and Table **3**. The changing trends in methane reaction rate versus temperature were rather similar to those in methane conversion versus temperature (Figure **8B**), and the $0.98Au_{0.98}Pt$/3DOM $CoCr_2O_4$ sample exhibited the highest specific reaction rate (4.56 μmol/(g_{cat} s), 939 μmol/(g_{Au} s), and 920 μmol/(g_{Pt} s)) at 340 °C (Table **3**). According to the XPS and H_2-TPR results (Figures **6** and **7** and Table **2**), we deduce that there was a synergistic effect between Au_yPt NPs and 3DOM $CoCr_2O_4$, and such a synergistic action would have an important role to play in the combustion of methane.

To probe the catalytic stability, we carried out the 40-h on-stream methane combustion over the $0.98Au_{0.98}Pt$/3DOM $CoCr_2O_4$ sample at 340 °C and SV = 20,000 mL/(g h), and the result is shown in Figure **9**. Apparently, there was no significant decrease in methane conversion within 40 h of on-stream methane combustion. That is to say, the $0.98Au_{0.98}Pt$/3DOM $CoCr_2O_4$ sample was catalytically stable under the adopted conditions.

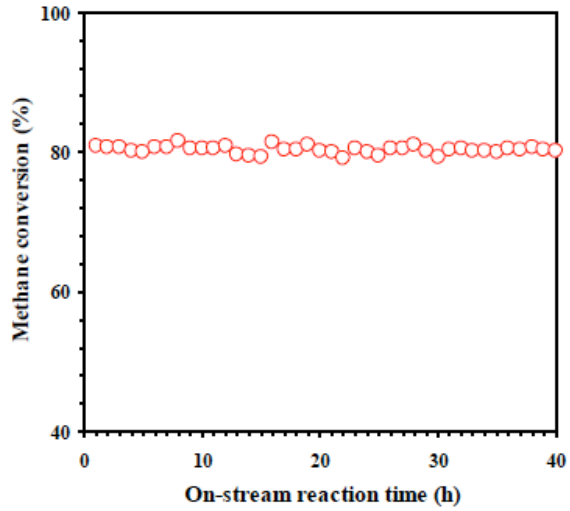

Figure 9: Methane conversion as a function of on-stream reaction time over the $0.98Au_{0.98}Pt$/3DOM $CoCr_2O_4$ sample at 340 °C and SV = 20,000 mL/(g h).

There have been a number of reports on the combustion of methane over various catalysts. Our $0.98Au_{0.98}Pt$/3DOM $CoCr_2O_4$ sample ($T_{90\%}$ = 402 °C at SV = 40,000 mL/(g h)) was much higher in catalytic performance to 4.5 wt% $Ru/ZnAl_2O_4$ ($T_{90\%}$ = 580 °C at SV = 32,000 h^{-1}) [41], similar to 1 wt% Pd/ZrO_2 ($T_{90\%}$ = 400 °C at SV = 35,000 mL/(g h)) [42], but lower than 3 wt% Pd-PdO_x-Pt/Al_2O_3 ($T_{90\%}$ = 327 °C at SV = 120,000 mL/(g h)) [16].

3.5. Effects of SV, Water Vapor, and Carbon Dioxide

The effect of SV on methane combustion over the $0.98Au_{0.98}Pt$/3DOM $CoCr_2O_4$ sample is shown in Figure **10**. It is observed that methane conversion decreased with the rise in SV, a result due to the shortening of contact time.

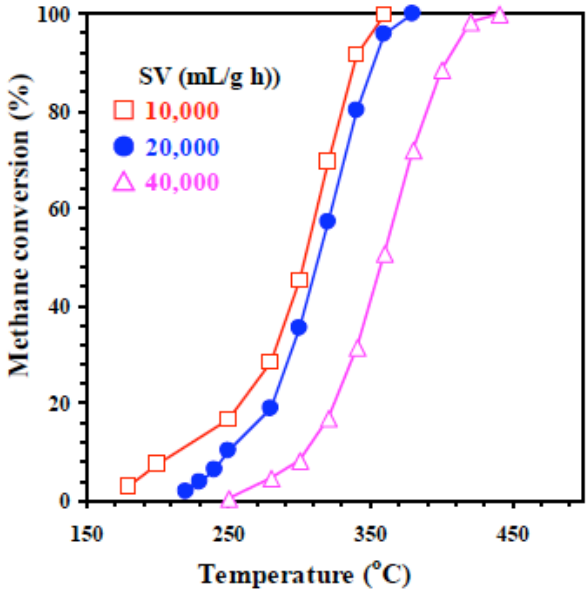

Figure 10: Effect of SV on methane combustion over the $0.98Au_{0.98}Pt$/3DOM $CoCr_2O_4$ sample.

On-stream methane combustion over the $0.98Au_{0.98}Pt$/3DOM $CoCr_2O_4$ sample in the presence and absence of 5.0 vol% water vapor or 2.5-5.0 vol% carbon dioxide at 380 °C and SV = 20,000 mL/(g h) was conducted to examine the effect of moisture or CO_2 on catalytic activity, and the result is shown in Figure **11**. It is found that when 5.0 vol% water vapor was introduced to the feedstock, methane conversion decreased from ca. 80 to 73%; when water vapor was cut off, methane conversion was restored to the original value in the absence of water vapor. The partial deactivation of the $0.98Au_{0.98}Pt$/3DOM $CoCr_2O_4$ sample

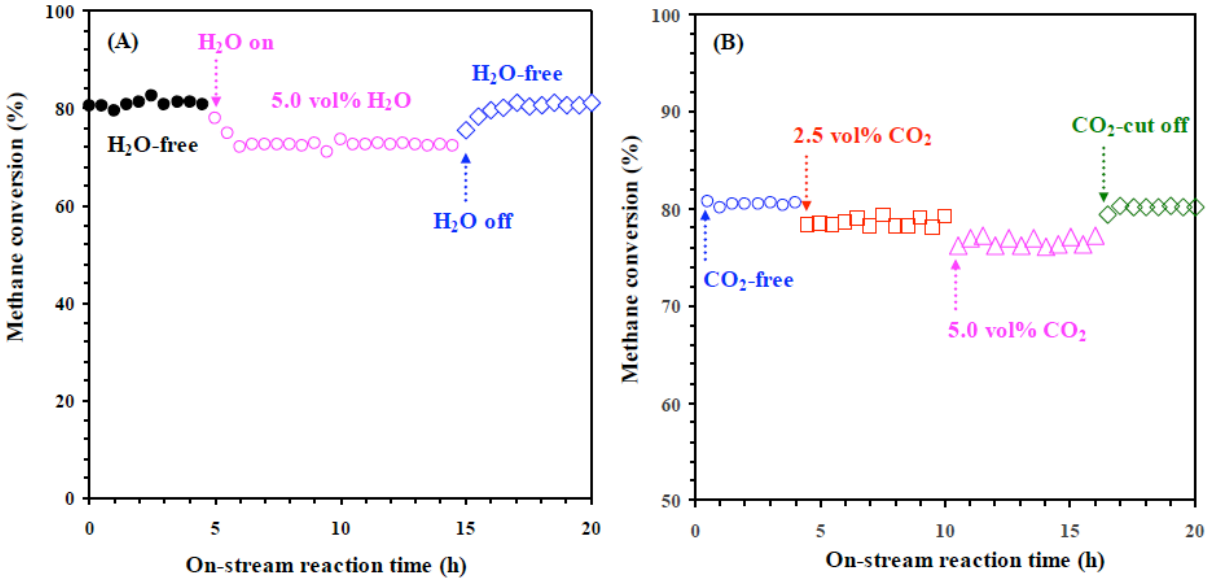

Figure 11: Effects of (A) water vapor and (B) CO_2 on methane conversion over the $0.98Au_{0.98}Pt$/3DOM $CoCr_2O_4$ sample at 340 °C and SV = 20,000 mL/(g h).

in the presence of 5.0 vol% water vapor might be due to the competitive adsorption of water and methane molecules on the surface of the sample, and such a partial deactivation was reversible. Similar phenomena have been reported by other researchers [8, 24, 25]. After adding 2.5 vol% CO_2 to the reaction system, methane conversion was decreased by ca. 2%; when CO_2 concentration was switched to 5.0 vol%, methane conversion was further decreased by ca. 2%. This result indicates that CO_2 was weakly adsorbed on the surface of the catalyst, causing the activity to decrease slightly. When 5.0 vol% CO_2 was cut off, methane conversion was recovered to the original value in the absence of CO_2, suggesting that the partial deactivation induced by CO_2 addition was also reversible.

CONCLUSIONS

The 3DOM $CoCr_2O_4$, 0.49Au/3DOM $CoCr_2O_4$, 0.48Pt/3DOM $CoCr_2O_4$, and $(0.49\text{-}1.92)Au_{0.98\text{-}1.01}Pt$/3DOM $CoCr_2O_4$ samples with a surface area of 32-35 m^2/g could be prepared using the PMMA-templating and PVA-protected reduction methods, respectively. The 3DOM $CoCr_2O_4$ in the samples was of a cubic spinel-type crystal phase and possessed a high-quality 3DOM structure. The noble metal NPs with an average size of 3-5 nm were highly dispersed on the surface of 3DOM $CoCr_2O_4$. Among these samples, $0.98Au_{0.98}Pt$/3DOM $CoCr_2O_4$ showed the highest O_{ads} species concentration and the best low-temperature reducibility, thus performing the best ($T_{50\%}$ = 315 °C and $T_{90\%}$ = 354 °C) for methane combustion at SV = 20,000 mL/(g h). The introduction of water vapor and carbon dioxide to the reaction system led to the partial deactivation of the $0.98Au_{0.98}Pt$/3DOM $CoCr_2O_4$ sample, and such a deactivation was reversible. Therefore, we conclude that the good catalytic activity of $0.98Au_{0.98}Pt$/3DOM $CoCr_2O_4$ was associated with its highly dispersed $Au_{0.98}Pt$ NPs, high O_{ads} species concentration, good low-temperature reducibility, and strong interaction between $Au_{0.98}Pt$ NPs and 3DOM $CoCr_2O_4$.

ACKNOWLEDGMENTS

This work was supported by the National Natural Science Foundation of China (21377008 and 21677004) and National High Technology Research and Development Program of China (2015AA034603).

REFERENCES

[1] Ercolino G, Stelmachowski P and Specchia S. Catalytic performance of Pd/Co_3O_4 on SiC and ZrO_2 open cell foams for the process intensification of methane combustion in lean conditions. Ind Eng Chem Res 2017; 56: 6625-6636. http://dx.doi.org/10.1021/acs.iecr.7b01087

[2] Clark NN, McKain DL, Johnson DR, Wayne WS, Li H, Akkerman V, *et al.* Pump-to-wheels methane emissions from the heavy-duty transportation sector. Environ Sci Technol 2017; 51: 968-976. http://dx.doi.org/10.1021/acs.est.5b06059

[3] Ercolino G, Stelmachowski P, Grzybek G, Kotarba A and Specchia S. Optimization of Pd catalysts supported on Co_3O_4 for low-temperature lean combustion of residual methane. Appl Catal B: Environ 2017; 206: 712-725. http://dx.doi.org/10.1016/j.apcatb.2017.01.055

[4] Chen JH, Shi WB, Zhang XY, Arandiyan H, Li DF, *et al.* Roles of Li^+ and Zr^{4+} cations in the catalytic performances of $Co_{1-x}M_xCr_2O_4$ (M = Li, Zr; *x* = 0-0.2) for methane combustion. Environ Sci Technol 2011; 45: 8491-8497. http://dx.doi.org/10.1021/es201659h

[5] Gelin P and Primet M. Complete oxidation of methane at low temperature over noble metal based catalysts: a review. Appl Catal B: Environ 2002; 39: 1-37. http://dx.doi.org/10.1016/S0926-3373(02)00076-0

[6] Hu LH, Peng Q and Li YD. Low-temperature CH_4 catalytic combustion over Pd catalyst supported on Co_3O_4 nanocrystals with well-defined crystal planes. ChemCatChem 2011; 3: 868-874. http://dx.doi.org/10.1002/cctc.201000407

[7] Xu J, Ouyang LK, Mao W, Yang XJ, Xu XC, Su JJ, *et al.* Operando and kinetic study of low-temperature, lean-burn methane combustion over a Pd/γ-Al_2O_3 catalyst. ACS Catal 2012; 2: 261-269. http://dx.doi.org/10.1021/cs200694k

[8] Tan W, Deng JG, Xie SH, Yang HG, Jiang Y, Guo GS, *et al.* $Ce_{0.6}Zr_{0.3}Y_{0.1}O_2$ nanorod supported gold and palladium alloy nanoparticles: high-performance catalysts for toluene oxidation. Nanoscale 2015; 7: 8510-8523. http://dx.doi.org/10.1039/C5NR00614G

[9] Nepak D and Darbha S. Selective aerobic oxidation of alcohols over Au-Pd/sodium titanate nanotubes. Catal Commun 2015; 58: 149-153. http://doi.org/10.1016/j.catcom.2014.09.018

[10] Chen MS, Kumar D, Yi CW and Goodman DW. The promotional effect of gold in catalysis by palladium-gold. Science 2005; 310: 291-293. http://dx.doi.org/10.1126/science.1115800

[11] Enache DI, Edwards JK, Landon P, Solsona-Espriu B, Carley AF, Herzing AA, *et al.* Solvent-free oxidation of primary alcohols to aldehydes using Au-Pd/TiO_2 catalysts. Science 2006; 311: 362-365. http://dx.doi.org/10.1126/science.1120560

[12] Persson K, Ersson A, Jansson K, Iverlund N and Järås SG. Influence of co-metals on bimetallic palladium catalysts for methane combustion. J Catal 2005; 231: 139-150 http://dx.doi.org/10.1016/j.jcat.2005.01.001

[13] Burch R and Loader PK. Investigation of Pt/Al_2O_3 and Pd/Al_2O_3 catalysts for the combustion of methane at low concentrations. Appl Catal B: Environ 1994; 1-2: 149-164. http://dx.doi.org/10.1016/0926-3373(94)00037-9

[14] Yamamoto H and Uchida H. Oxidation of methane over Pt and Pd supported on alumina in lean-burn natural-gas engine exhaust. Catal Today 1998; 45: 147-151. http://doi.org/10.1016/S0920-5861(98)00265-X

[15] Narui K, Yata H, Furuta K, Nishida A, Kohtoku Y and Matsuzaki T. Effects of addition of Pt to PdO/Al_2O_3 catalyst on catalytic activity for methane combustion and TEM observations of supported particles, Appl Catal A: Gen 1999; 179: 165-173. http://doi.org/10.1016/S0926-860X(98)00306-8

[16] Kinnunen NM, Hirvi JT, Suvanto M and Pakkanen TA. Methane combustion activity of Pd-PdO_x-Pt/Al_2O_3 catalyst: The role of platinum promoter. J Mol Catal A: Chem 2012; 356: 20-28. http://doi.org/10.1016/j.molcata.2011.12.023

[17] Castellazzi P, Groppi G and Forzatti P. Effect of Pt/Pd ratio on catalytic activity and redox behavior of bimetallic Pt-Pd/Al_2O_3 catalysts for CH_4 combustion. Appl Catal B: Environ 2010; 95: 303-311. http://doi.org/10.1016/j.apcatb.2010.01.008

[18] Corro G, Cano C and Fierro JLG. A study of Pt-Pd/γ-Al_2O_3 catalysts for methane oxidation resistant to deactivation by sulfur poisoning. J Mol Catal A: Chem 2010; 315: 35-42. http://doi.org/10.1016/j.molcata.2009.08.023

[19] Hu JH, Zhao WY, Hu RS, Chang GY, Li C and Wang LJ. Catalytic activity of spinel oxides $MgCr_2O_4$ and $CoCr_2O_4$ for methane combustion. Mater Res Bull 2014; 57: 268-273. http://doi.org/10.1016/j.materresbull.2014.06.001

[20] Chen JH, Zhang XY, Arandiyan H, Peng Y, Chang HZ, Li JH. Low temperature complete combustion of methane over cobalt chromium oxides catalysts. Catal Today 2013; 201: 12-18. http://doi.org/10.1016/j.cattod.2012.03.026

[21] Wang ZW, Deng JG, Liu YX, Yang HG, Xie SH, Wu ZX, *et al.* Three-dimensionally ordered macroporous $CoCr_2O_4$-supported Au-Pd alloy nanoparticles: Highly active catalysts for methane combustion. Catal Today 2017; 281: 467-476. http://dx.doi.org/10.1016/j.cattod.2016.05.035

[22] Li XW, Dai HX, Deng JG, Liu YX, Xie SH, Zhao ZX, *et al.* Au/3DOM $LaCoO_3$: High-performance catalysts for the oxidation of carbon monoxide and toluene. Chem Eng J 2013; 228: 965-975. http://doi.org/10.1016/j.cej.2013.05.070

[23] Wei YC, Liu J, Zhao Z, Chen YS, Xu CM, Duan AJ, *et al.* Highly active catalysts of gold nanoparticles supported on three-dimensionally ordered macroporous $LaFeO_3$ for soot oxidation. Angew Chem Int Ed 2011; 50: 2326-2329. http://doi.org/10.1002/anie.201006014

[24] Xie SH, Deng JG, Zang SM, Yang HG, Guo GS, Arandiyan H, *et al.* Au-Pd/3DOM Co_3O_4: Highly active and stable nanocatalysts for toluene oxidation. J Catal 2015; 322: 38-48. http://doi.org/10.1016/j.jcat.2014.09.024

[25] Xie SH, Deng JG, Liu YX, Zhang ZH, Yang HG, Jiang Y, *et al.* Excellent catalytic performance, thermal stability, and water resistance of 3DOM Mn_2O_3-supported Au-Pd alloy nanoparticles for the complete oxidation of toluene. Appl Catal A: Gen 2015; 507: 82-90. http://doi.org/10.1016/j.apcata.2015.09.026

[26] Liotta LF, Di Carlo G, Pantaleo G, Venezia AM and Deganello G. Co_3O_4/CeO_2 composite oxides for methane emissions abatement: Relationship between Co_3O_4-CeO_2 interaction and catalytic activity. Appl Catal B: Environ 2006; 66: 217-227. http://doi.org/10.1016/j.apcatb.2006.03.018

[27] Feng YJ, Li L, Niu SF, Qu Y, Zhang Q, Li YS, *et al.* Controlled synthesis of highly active mesoporous Co_3O_4 polycrystals for low temperature CO oxidation. Appl Catal B: Environ 2012; 111-112: 461-466. http://doi.org/10.1016/j.apcatb.2011.10.035

[28] Lin YX, Cai WP, Tian XY, Liu XL, Wang GZ and Liang CH. Polyacrylonitrile/ferrous chloride composite porous nanofibers and their strong Cr-removal performance. J Mater Chem 2011; 21: 991-997. http://doi.org/10.1039/C0JM02334E

[29] Xie XW, Li Y, Liu ZQ, Haruta M and Shen WJ. Low-temperature oxidation of CO catalysed by Co_3O_4 nanorods. Nature 2009; 458: 746-749. http://doi.org/10.1038/nature07877

[30] Kim DC and Ihm SK. Application of spinel-type cobalt chromite as a novel catalyst for combustion of chlorinated organic pollutants. Environ Sci Technol 2001; 35: 222-226. http://doi.org/10.1021/es001098k

[31] Sloczynski J, Janas J, Machej T, Rynkowski J and Stoch J. Catalytic activity of chromium spinels in SCR of NO with NH_3. Appl Catal B: Environ 2000; 24: 45-60. http://doi.org/10.1016/S0926-3373(99)00093-4

[32] Rousseau S, Loridant S, Delichere P, Boreave A, Deloume JP and Vernoux P. $La_{(1-x)}Sr_xCo_{1-y}Fe_yO_3$ perovskites prepared by sol-gel method: Characterization and relationships with catalytic properties for total oxidation of toluene. Appl Catal B: Environ 2009; 88: 438-447. http://doi.org/10.1016/j.apcatb.2008.10.022

[33] Ponce S, Peña MA and Fierro JLG. Surface properties and catalytic performance in methane combustion of Sr-substituted lanthanum manganites, Appl Catal B: Environ 2000; 24: 193-205. http://doi.org/10.1016/S0926-3373(99)00111-3

[34] Liu YX, Dai HX, Deng JG, Zhang L, Gao BZ, Wang Y, *et al.* PMMA-templating generation and high catalytic performance of chain-like ordered macroporous $LaMnO_3$ supported gold nanocatalysts for the oxidation of carbon monoxide and toluene. Appl Catal B: Environ 2013; 140-141: 317-326. http://doi.org/10.1016/j.apcatb.2013.04.025

[35] Zhao XT, Liu YX, Deng JG, Yang J, Zhang KF, Han Z, *et al.* Mesoporous Pd_xPt alloys: High-performance catalysts for methane combustion. Mol Catal 2017; 442: 191-201. http://doi.org/10.1016/j.mcat.2017.09.002

[36] Liu YX, Dai HX, Deng JG, Li XW, Wang Y, Arandiyan H, *et al.* Au/3DOM $La_{0.6}Sr_{0.4}MnO_3$: Highly active nanocatalysts for the oxidation of carbon monoxide and toluene. J Catal 2013; 305: 146-153. http://doi.org/10.1016/j.jcat.2013.04.025

[37] Grzybowska B, Sloczynski J, Grabowski R, Wcislo K, Kozlowska A, Stoch J, *et al.* Chromium oxide/alumina catalysts in oxidative dehydrogenation of isobutane. J Catal 1998; 178: 687-700. http://doi.org/10.1006/jcat.1998.2203

[38] Bracconi P and Dufour LC. Hydrogen reduction of cobalt-chromium spinel oxides. II. Cobalt chromite ($CoCr_2O_4$)-cobalt oxide (Co_3O_4) solid solutions. J Phys Chem 1975; 79: 2400-2405. http://doi.org/10.1021/j100589a011

[39] Chen KD, Xie SB, Bell AT and Iglesia E. Structure and properties of oxidative dehydrogenation catalysts based on MoO_3/Al_2O_3. J Catal 2001; 198: 232-242. http://doi.org/10.1006/jcat.2000.3125

[40] Wu ZX, Deng JG, Liu YX, Xie SH, Jiang Y, Zhao XT, *et al.* Three-dimensionally ordered mesoporous Co_3O_4-supported Au-Pd alloy nanoparticles: High-performance catalysts for methane combustion. J Catal 2015; 332: 13-24. http://doi.org/10.1016/j.jcat.2015.09.008

[41] Okal J, Zawadzki M and Baranowska M. Thermal treatment in air of the $Ru/ZnAl_2O_4$ catalysts for the methane combustion. Appl Catal A: Gen 2014; 471: 98-105. http://dx.doi.org/10.1016/j.apcata.2013.11.034

[42] Yang SW, Maroto-Valiente A, Benito-Gonzalez M, Rodriguez-Ramos I and Guerrero-Ruiz A. Methane combustion over supported palladium catalysts: I. Reactivity and active phase. Appl Catal B: Environ 2000; 28: 223-233. http://doi.org/10.1016/S0926-3373(00)00178-8

Received on 25-01-2017 Accepted on 07-12-2017 Published on 21-12-2017

DOI: http://x.doi.org/10.15377/2410-3624.2017.04.3